COBEM 2023 27TH INTERNATIONAL CONGRESS OF MECHANICAL ENGENEERING

ABCM Brazilian Society of Mechanical Sciences and Engineering
27th ABCM International Congress of Mechanical Engineering
December 04-08, 2023, Florianópolis-SC, Brazil

COB-2023-1271
FAULT DETECTION IN BEARINGS BASED ON CONVOLUTIONAL NEURAL NETWORKS USING LOW-COST MEMS ACCELEROMETERS

Lucas Almeida Willenshofer
Federal Institute of São Paulo, São Paulo, SP, Brazil.
lucaswillenshofer@gmail.com

Caique Movio Pereira de Souza
Mackenzie Presbyterian Institute, São Paulo, SP, Brazil.
caiquemovio@gmail.com

Rogério Daniel Dantas
Federal Institute of São Paulo, São Paulo, SP, Brazil.
rogerio.dantas@ifsp.edu.br

Rene Ramos de Oliveira
Nuclear and Energy Research Institute, São Paulo, SP, Brazil.
rolivier@ipen.br

Vanessa Seriacopi
Maua Institute of Technology, Maua, SP, Brazil.
vanessa.seriacopi@maua.br

Wilson Carlos da Silva Junior
Federal Institute of São Paulo, São Paulo, SP, Brazil.
wilsoncarlos@ifsp.edu.br

Abstract. *The study focuses on detecting bearing failures in industrial environments, which are crucial to equipment performance and reliability. Commercial accelerometers used for fault signal acquisition are expensive, limiting their implementation in serial equipment. Convolutional neural networks (CNN) have emerged as an emerging method for fault detection, but this method does not work well with one-dimensional data. To address this, the study proposes evaluating two low-cost microelectromechanical systems (MEMS) accelerometers for obtaining vibration signals and converting them into 2D images for CNN analysis. An experimental platform was built, connecting the MPU6050 and ADXL345 accelerometers to bearings with normal and faulty conditions. Vibration signature images were inserted into CNN with dimensions of 16x16, 22x22, and 28x28 to assess their impact on accuracy. The results showed that the proposed algorithm achieved high accuracy: for MPU6050, 97,31% accuracy with 16x16 images, 96,95% with 22x22 and 98,92% with 28x28, for ADXL345, 98,31% with 16x16 images, 99,70% with 22x22 and 99,82% with 28x28. This research demonstrates the effectiveness of low-cost accelerometers and 2D image conversion to improve bearing failure detection.*

Keywords: *Convolutional neural network; low-cost MEMS accelerometer; bearing failure detection.*

1. INTRODUCTION

In modern industries, rotating machines represent over 90% of the equipment used (HAN et al., 2021). Rotating machines encompass a wide variety of equipment such as motors, compressors, mechanical spindles, and mechanical transmission boxes (YI et al., 2020). Being one of the main machine elements that make up a rotating machine, the bearing is intended to support axial and radial loads, as well as to reduce rotational friction with the shaft (WANG et al., 2019).

In general, rotating machines are used for long periods and in complex and variable workload environments, because of this, bearings are constantly subject to early mechanical wear (DEVECI et al., 2021). This characteristic makes bearings identified as a critical element representing approximately 55% of failures in rotating machines (DUAN et al., 2019). When bearings fail unexpectedly, they can cause significant damage to the equipment, with high repair and replacement costs, in addition to causing production stoppages, directly impacting the operational efficiency of the equipment, causing significant economic losses for companies (DEVECI et al., 2021). Therefore, to ensure greater reliability of rotating machines, the monitoring of rolling bearings is of great importance, for which it is necessary to use accurate and fast methods for diagnosing the real state of the equipment.

Despite the wide range of approaches that can be used in applications to monitor the state of equipment, the analysis of vibration signals is the most used technique to determine the mechanical the machine, as this is one of the first symptoms of perceived degradation, it is usually followed by noise, heat and finally smoke (EULDJI et al., 2021). The development of low-cost technology in the manufacture of micro-electro-mechanical systems (MEMS) has spread the use of this type of sensor for the analysis of vibration signals (ASWIN et al., 2020).

Given the relevance, the theme of this work arises from the proposal to evaluate and compare the use of low-cost MEMS-type accelerometers applied to the prediction of rolling element defects and outer race defects in bearings.

2. CONVOLUTIONAL NEURAL NETWORKS

Inspired by the visual cortices of animals, Convolutional Neural Networks (CNNs) have gained a great deal of attention in recent years. The convolution operation is performed for the first time to detect patterns in images ranging from simple features like edges and corners to complex features. Specifically, lower levels in the network detect fundamental lower-level visuals; and the overlapping layers detect higher-level features, which are built on lower levels (ZHANG et al., 2020).

CNNs are a type of neural network designed to process high-dimensional data in the form of spatial matrices, such as time series (1D) or images (2D). They are called convolutional because they use the mathematical operation of convolution in at least one of their layers (LECUN et al., 2015). Convolution is a mathematical operation that allows you to extract features from a dataset through a fixed-size window that is slid over the data. This allows the network to capture patterns at different scales and resolutions, which is particularly useful when processing images and other spatial data (ZHANG et al., 2020). Typical CNN usually consists of the input layer, convolutional layer, pooling layer, fully connected layer, and output layer (DI et al., 2020).

For the application of convolutional networks in the creation of bearing fault extractors, mainly the 1D temporal raw data obtained from accelerometers are first stacked to the 2D vector, which is passed to a convolutional layer for feature generation, then by a pooling layer for vector reduction. The combination of this convolution and pooling pattern is repeated many times to further extend the network. The output of the hidden layers will be delivered to one or several fully connected layers, the result of which is transferred to a top classifier based on softmax or sigmoid functions to determine if a bearing fault is present (ZHANG et al., 2020). The basic architecture of a CNN-based bearing fault classifier is illustrated in Figure 1.

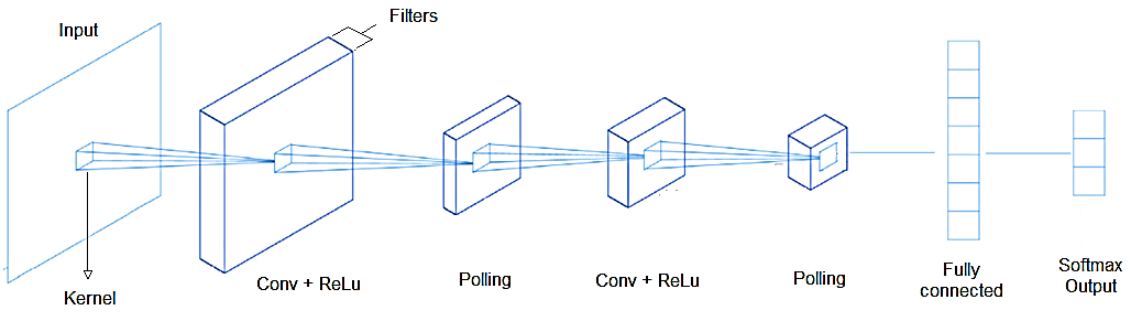

Figure 1. The basic architecture of a CNN-based bearing fault classifier.

The units in a convolution layer are organized into feature maps, within which each unit is connected to local patches in the previous layer's feature maps through a set of weights called a convolution filter. Usually, the convolutional operation is followed by a non-linear activation function that adds non-linearity to the system, such as ReLU (rectified linear unit). Pooling layers act as a dimensionality reduction mechanism, the most common pooling functions are maximum pooling and average pooling, which are applied to the filter convolution output. The fully connected layer is the layer with the most training parameters in CNN, it converts all the two-dimensional feature maps obtained by convolution into a one-dimensional feature vector as input to the classifier, the last layer of CNN is the output layer, responsible for perform the final classification of the data. (DI et al., 2020).

3. MATERIALS AND METHODS

The experimental bench to be used was made on the campus of the Federal Institute of Education, Science, and Technology of São Paulo, and has some materials donated by partner companies CESTARI-WEG and Schneider Electric, the bench has a gearmotor connected to two bearings through an elastic coupler and machined 1020 steel shaft. Figure 2 shows the workbench and the elements that compose it.

The geared motor used has a 3 HP three-phase induction motor with a nominal speed of 1780 RPM connected to the reduction input, the internal gear arrangement provides a reduction of 48.90 times resulting in an output speed of 36.8

RPM with 400 Nm of torque when the engine is at rated speed. To allow the collection of data in different conditions of use, the experimental bench has a control panel with a frequency inverter allowing the variation of motor rotation, as well as the selection of the direction of rotation.

For carrying out the experiments, four NSK spherical roller bearings, model 21306CD, were used. This specific bearing has as its main features a high operating load capacity, pressed steel cage, and permissible misalignment between 1º and 2.5º in normal load situations. Of the four bearings chosen for the study, two remained unchanged, maintaining their original characteristics. The other two were segregated for manual insertion of defects, one bearing for roller defect and one bearing for outer race defect, respectively.

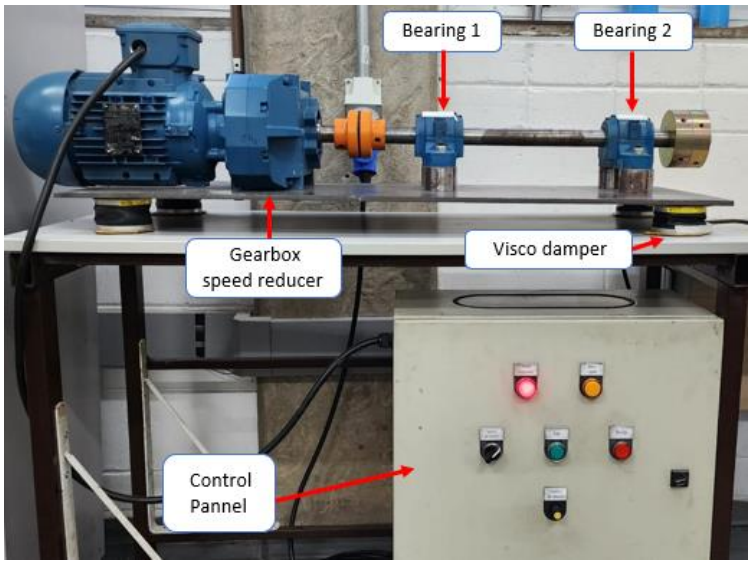

Figure 2. Experimental bench.

Figure 3 shows the open bearings coupled to the driven shaft, is possible to notice that the top of the cover of each bearing was milled to facilitate the subsequent assembly of the accelerometers.

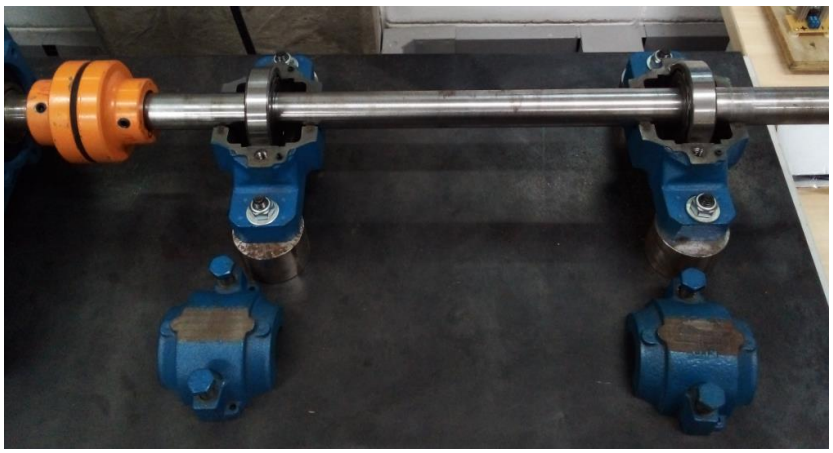

Figure 3. Mechanical assembly of bearings on the experimental bench.

For this experiment, the sensors chosen were the accelerometers MPU6050 and ADXL345, given their low cost (US $10 and US $5 respectively) and easy application due to their already digitized outputs. Both are MEMS-type triaxial accelerometers that can be adjusted by the user via programming to operate at ±2g, ±4g, ±8g, and ±16g. Table 1 shows a comparison between the main characteristics of the MPU6050 and ADXL345 accelerometers.

Table 1. Comparison between MPU6050 and ADXL345

Features	**MPU6050**	**ADXL345**
Price	US $10	US $10
Power supply	3.3 to 5 V	3.3 to 5V
Supply voltage	500 uA	140 uA
Non-linearity	0.2%	0.5%
Operating temperature	-40 to +85 ºC	-40 to +85 ºC
Communication interface	I²C	I²C

As the communication interface of the accelerometers takes place through the I²C serial, it is necessary to use a controller that can perform the readings, for which the ESP-32 microcontroller was chosen due to its low market cost and sufficient performance for the application. To minimize possible interference between the microcontroller and the accelerometer as much as possible, it was decided to solder the accelerometer to a standard island-type board and connect the microcontroller to this board through a socket.

To attach the microcontroller/sensor assembly to the bearing, a box with a base magnetized by neodymium magnets was developed and printed in 3D. Figure 4 shows the printed case and the accelerometer soldered to the island board with and without the microcontroller fitted.

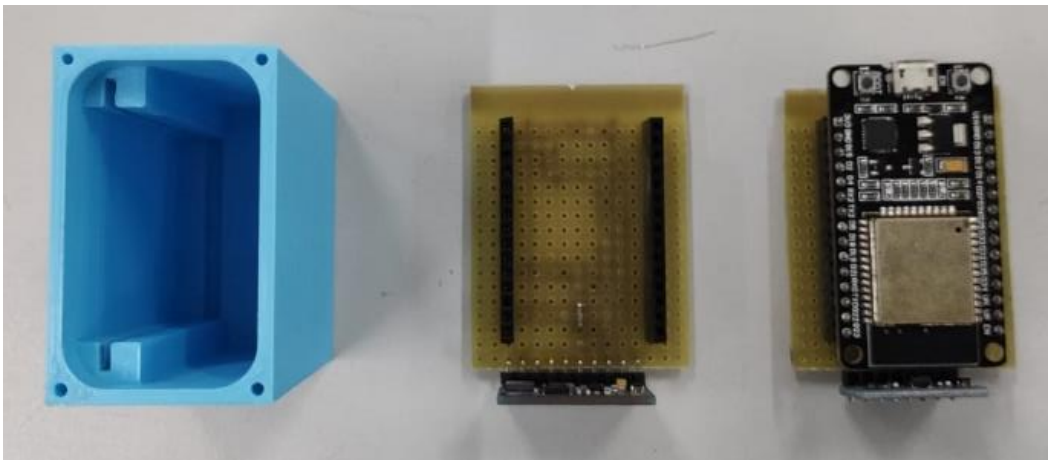

Figure 4. Printed case and the accelerometer soldered to the island board with and without the microcontroller fitted.

Finally, Figure 5 shows the set mounted on the case coupled to the accelerometer during an acquisition.

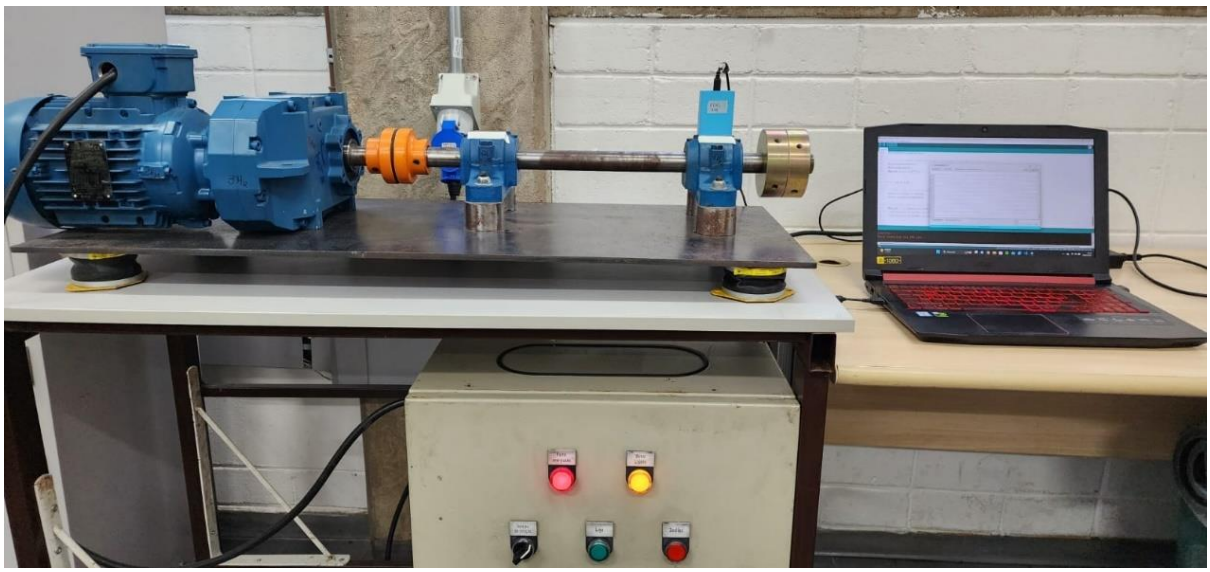

Figure 5. Sensor connected to the bearing during an acquisition.

For signal acquisition, bearing 1 always used the sample in good condition, and bearing 2 varied between samples in good condition, roller defect, and outer race defect. Four shaft rotation speeds were used for each bearing sample 2, being obtained when the inverter was set at 45, 60, 75, and 90 Hz. Table 2 shows a summary of all twelve combinations of acquisition scenarios set by default.

Table 2. Scenarios for signal acquisition.

Acquisition scenario	Inverter frequency (Hz)	Output rotation (RPM)	Bearing 2 condition
1	45	27.8	Good
2	60	36.7	Good
3	75	46.0	Good
4	90	54.8	Good
5	45	27.8	Roller defect
6	60	36.7	Roller defect
7	75	46.0	Roller defect
8	90	54.8	Roller defect
9	45	27.8	Outer race defect
10	60	36.7	Outer race defect
11	75	46.0	Outer race defect
12	90	54.8	Outer race defect

For the data to be acquired in the most uniform way possible, an experimental procedure for data collection was also developed, allowing all measurements were always carried out in the same order of execution for both sensors in all speed ranges. Table 3 shows the experimental procedure adopted.

Table 3. Experimental procedure for signal acquisition on the experimental bench.

Step	Task
1	30 minutes warm-up
2	Set inverter to LSP=45 and HSP=60
3	Collect data counterclockwise at 45 Hz with the ADXL345 accelerometer for 30 min and save
4	Collect data counterclockwise at 60 Hz with the ADXL345 accelerometer for 30 min and save
5	Set inverter to LSP=75 and HSP=90
6	Collect data counterclockwise at 75 Hz with the ADXL345 accelerometer for 30 min and save
7	Collect data counterclockwise at 90 Hz with the ADXL345 accelerometer for 30 min and save
8	Change the sensor
9	Collect data counterclockwise at 90 Hz with the MPU6050 accelerometer for 30 min and save
10	Collect data counterclockwise at 75 Hz with the MPU6050 accelerometer for 30 min and save
11	Set inverter to LSP=45 and HSP=60
12	Collect data counterclockwise at 60 Hz with the MPU6050 accelerometer for 30 min and save
13	Collect data counterclockwise at 45 Hz with the MPU6050 accelerometer for 30 min and save
14	Change the bearing 2 sample and repeat the tests

In Figure 6, a temporal vibration signal can be seen in a 10-second window obtained through the signals collected by the MPU6050 accelerometer for the three respective bearing samples.

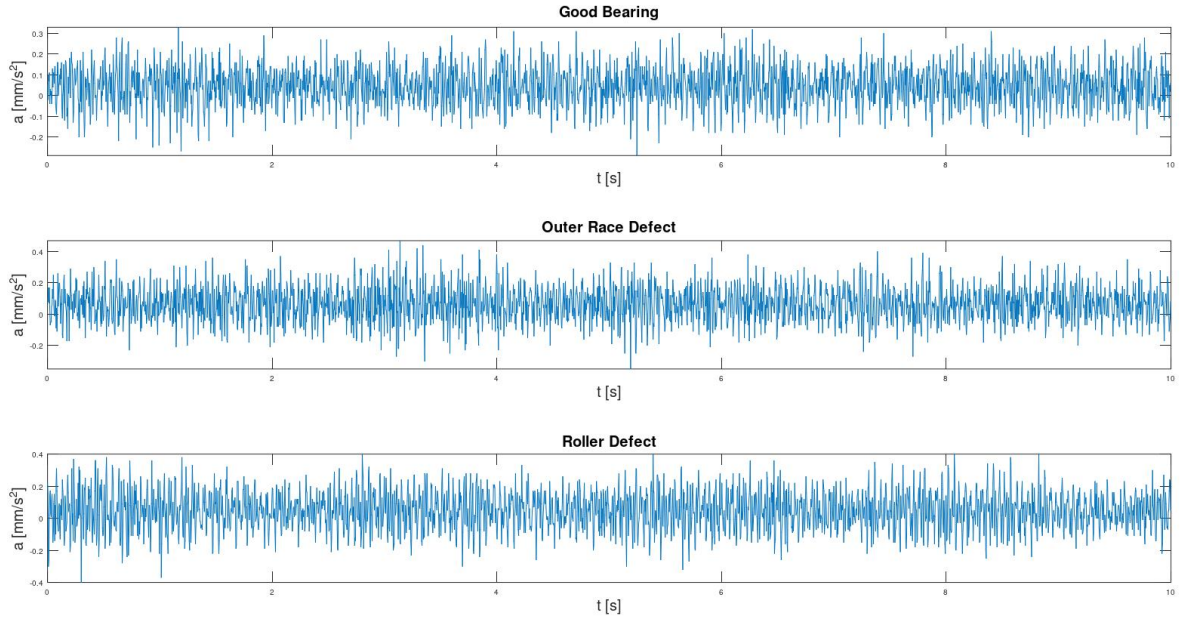

Figure 6. Vibration signal acquired by the MPU6050 sensor for the three bearing samples.

To extract the maximum performance from the network algorithm, the temporal data of one dimension were converted into vectors of two dimensions in grayscale. To convert temporal data into images, they were first normalized to values between 0 and 1 and then grouped into a 2D matrix (SAYED et al., 2023).

For the pixels to be grouped, the signal must be windowed using a specific length to be determined by the number of pixels needed to obtain the image. this offset can be greater than, less than, or equal to the window length and is user-defined.

For the present work, the temporal signals were converted to three dimensions of predefined images, to compare the influence of image dimensionality on the accuracy of the algorithm. Table 4 shows the dimensions, the window length, and the step adopted for each of the defined image dimensions, as well as the total size of the dataset with the data collected by the accelerometers.

Table 4. Dimensions, window length, stride, and number of images for data collected with accelerometers.

Accelerometer	Image size	window length	Stride	Number of images generated
MPU6050	28x28	784	500	16434
MPU6050	22x22	484	390	21070
MPU6050	16x16	256	200	41089
ADXL345	28x28	784	500	23290
ADXL345	22x22	484	390	29861
ADXL345	16x16	256	200	58232

Figure 7 shows an example of 3 samples of the images converted through the vibration signals collected by the MPU6050 accelerometer, with the images named PE referring to the acquisition performed on the defective bearing in the outer race, the images denominated R referring to images acquired in the defective bearing of roller and images called N referring to the acquisition carried out on the bearing in good condition.

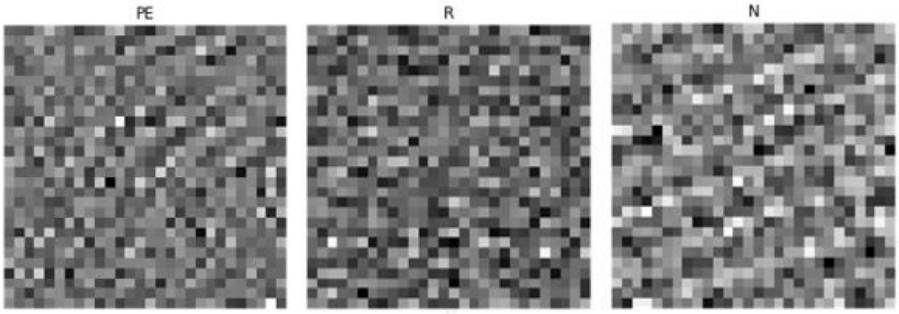

Figure 7. Sample of images with dimensions of 28x28 converted through vibration signals obtained by the MPU6050 sensor.

In the adopted convolutional network configuration, the first layer added is a convolutional layer with 32 filters and a kernel size of 3x3, with the ReLU activation function. The input of the convolutional layer is defined by the size of the image that enters the algorithm. The second layer added is a maximum pooling layer with a 2x2 window and a 2x2 step responsible for reducing the image dimension. The third layer added is another convolutional layer with 64 filters and a kernel size of 3x3, with the ReLU activation function. The fourth layer added is another maximum pooling layer with a 2x2 window and a 2x2 pitch, responsible for again reducing the image dimension. The fifth layer added is a flattened layer, which transforms the output of the previous layer into a one-dimensional vector. The added sixth layer is a fully connected dense layer with 128 neurons and the ReLU activation function. The seventh and last layer added is another dense layer with 3 neurons (equal to the number of classes N, R, and PE), and the Softmax activation function to generate the probabilities of each class. Table 5 shows the structure of the configuration.

Table 5. The parameters of the constructed CNN.

Layer	Type	Neurons / Filters	Kernel	Activation function
1	Conv2D	32	(3.3)	ReLU
2	MaxPooling2D	-	(2.2)	-
3	Conv2D	64	(3.3)	ReLU
4	MaxPooling2D	-	(2.2)	-
5	Flatten	-	-	-
6	Dense	128	-	ReLU
7	Dense	3	-	Softmax

The batch size was set to 200, which means that the model updates the weights after every batch of 200 training examples. The number of epochs was set to 20, which means that the model will run through the entire training dataset 20 times. Training data were randomized before each epoch. The configuration was compiled with the categorical cross-entropy loss function and the Adam optimizer.

4. RESULTS AND DISCUSSIONS

The proposed network configuration was tested for the classification of failures in bearings taking as input the 16x16, 22x22, and 28x28 images generated through the data collected by the accelerometers MPU6050 and ADXL345.

Figure 8 shows the results of network training for fault classification with 28x28 images from the MPU6050 accelerometer. In blue is the training curve and in orange is the validation curve both as a function of the number of epochs. it can be observed that the accuracy of the model increases rapidly in the first epochs, in addition, the accuracy in the validation set closely follows the accuracy in the training set, indicating that the model is not suffering from overfitting, this pattern was repeated for the other samples tested.

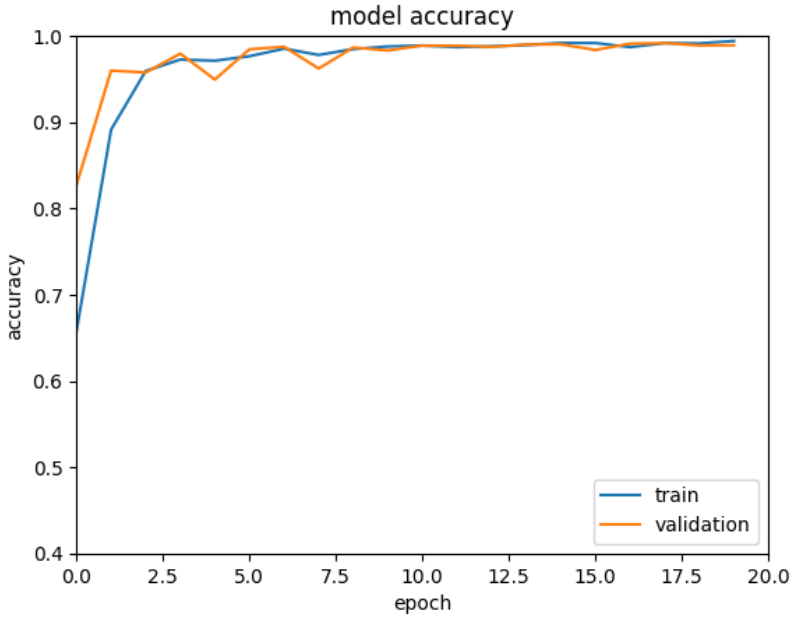

Figure 8. Model accuracy using 28x28 images generated from data collected by the MPU 6050 accelerometer.

Figure 9 presents a graphical view of the confusion matrices for 28x28, 22x22, and 16x16 images obtained through the signals of both accelerometers, it appears that most of the model's predictions are located on the main diagonal, which indicates that the model correctly classified most of the samples in the dataset. Furthermore, except for the confusion matrix presented in Figure B, the PE class is lighter than the other areas, indicating that the model had the highest success rate for this class. Through the matrices, it can also be observed that for both accelerometers, the larger the image size, the more accurate the classification.

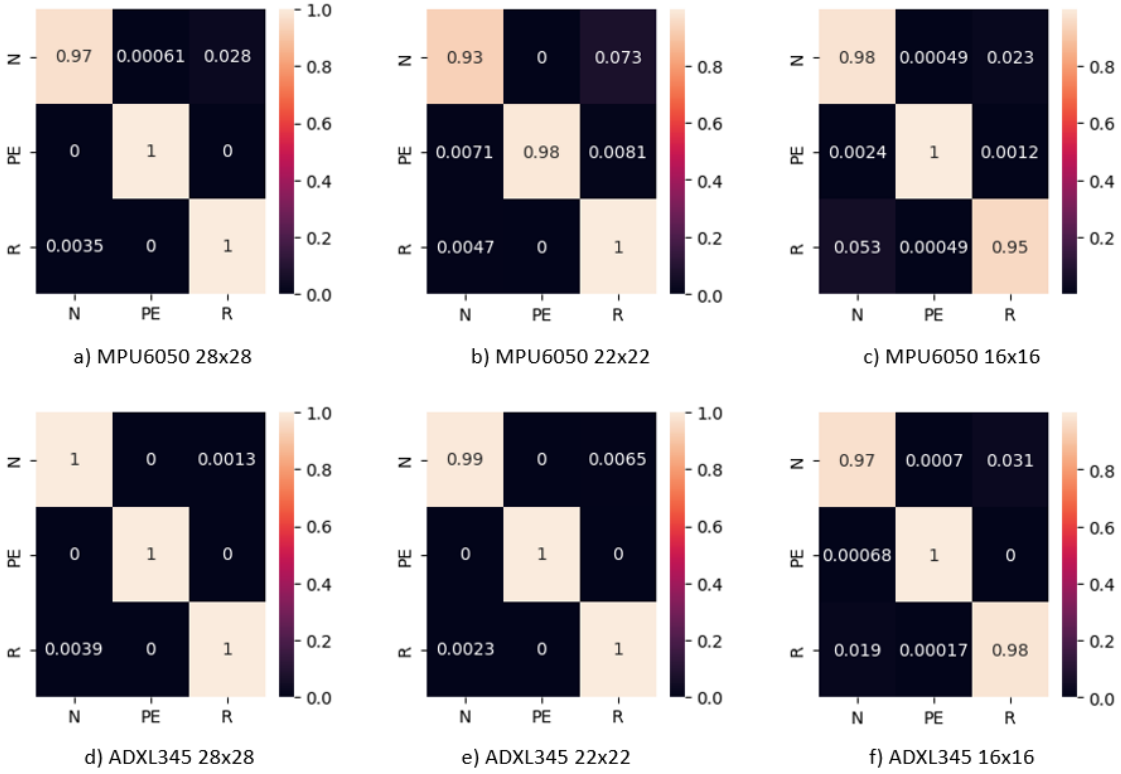

Figure 9. The confusion matrix for the fault diagnosis results.

Table 6 shows the accuracy of both accelerometers for the different dimensions of the tested images, it can be noted that both sensors showed promising results, it is also possible to observe that despite being cheaper, the ADXL345 accelerometer performed better when compared to the MPU6050 under the same conditions.

Table 6. The accuracy obtained with the adopted network configuration.

Accelerometer	Image dimension	Train data accuracy (%)	Test data accuracy (%)
MPU6050	28x28	99.29	98.92
MPU6050	22x22	97.74	96.95
MPU6050	16x16	97.96	97.31
ADXL345	28x28	100	99.82
ADXL345	22x22	100	99.70
ADXL345	16x16	99.98	98.31

5. CONCLUSION

In conclusion, this study highlights the importance of detecting bearing faults in the industrial field and addresses the limitations of expensive commercial accelerometers by proposing the use of low-cost MEMS accelerometers. By converting the obtained vibration signals into 2D images and applying convolutional neural networks (CNN), the proposed algorithm effectively identifies and classifies subtle characteristics of bearing signals. The experimental results demonstrate high accuracy across different image dimensions, showcasing the potential of this approach. The research provides valuable insights into the feasibility of implementing cost-effective fault detection methods in serial equipment. By enabling more accessible and reliable fault detection, this study contributes to improving the performance and reliability of mechanical equipment in various industrial applications. The findings encourage further exploration of low-cost sensor technologies and their integration with advanced machine-learning techniques for enhanced fault detection and preventive maintenance strategies in the industry.

In future works, this type of approach has the potential to be applied in the detection of other types of failures in mechanical systems, such as, for example, the detection of failures in gear sets and the detection of misalignments in rotating equipment, in these cases it should prior training with the data of the respective expected failures should be carried out, to provide parameters for the machine learning of these new failure modes. It is also possible to highlight the possibility of implanting the learning algorithm already pre-trained in low-cost microprocessors (tinyML), allowing the diagnosis to be made locally without the need to process information in a cloud server, thus replacing the excessive sending of raw data to the server by the result of the equipment diagnostics.

6. REFERENCES

Aswin, F.; Dwisaputra, I.; Afriansyah, R. *Online vibration monitoring system for rotating machinery based on 3-axis MEMS accelerometer.* Journal of Physics: Conference Series, v. 1450, n. 1, 2020. DOI: 10.1088/1742-6596/1450/1/012109.

Deveci, B.U.; Celtikoglu, M.; Alp, T.; Albayrak, O.; Unal, P.; Kirci, P. *A comparison of deep transfer learning methods on bearing fault detection.* Proceedings - 2021 International Conference on Future Internet of Things and Cloud, FiCloud 2021, p. 285–292, 2021. DOI: 10.1109/FiCloud49777.2021.00048.

Di, W.; Ren, Y.; Xuyang, X.; Tianshu, W.; Qiao, P.; Yusheng, C. *Fault diagnosis method for bearing and gear based on deep learning waveform image recognition.* Proceedings - 2020 7th International Conference on Information Science and Control Engineering, ICISCE 2020, p. 622–628, 2020. DOI: 10.1109/ICISCE50968.2020.00134.

Duan, J.; Shi, T.; Zhou, H.; Duan, J.; Xuan, J.; Zhang, J. *A novel bearing health prognostic method based on time-frequency analysis and LSTM*. 2019 Prognostics and System Health Management Conference, PHM-Qingdao 2019, n. 51575202, 2019. DOI: 10.1109/PHM-Qingdao46334.2019.8942821.

Euldji, R.; Boumahdi, M.; Bachene, M. *Decision-making based on decision tree for ball bearing monitoring*. 2020 2nd International Workshop on Human-Centric Smart Environments for Health and Well-Being, IHSH 2020, p. 171–175, 2021. DOI: 10.1109/IHSH51661.2021.9378734.

Han, T.; Zhang, L.; Yin, Z.; Tan, A.C.C. *Rolling bearing fault diagnosis with combined convolutional neural networks and support vector machine*. Measurement: Journal of the International Measurement Confederation, v. 177, n. December 2020, p. 109022, 2021. DOI: 10.1016/j.measurement.2021.109022.

Lecun, Y.; Bengio, Y.; Hinton, G. *Deep learning. nature*, v. 521, n. 7553, p. 436–444, 2015. DOI: 0.1038/nature14539.

Sayed, A.N.; Himeur, Y.; Bensaali, F. *From time-series to 2D images for building occupancy prediction using deep transfer learning*. Engineering Applications of Artificial Intelligence, v. 119, n. December 2022, p. 105786, 2023. DOI: 10.1016/j.engappai.2022.105786.

Wang, J.; Mo, Z.; Zhang, H.; Miao, Q. *A deep learning method for bearing fault diagnosis based on time-frequency image.* IEEE Access, v. 7, p. 42373–42383, 2019. DOI: 10.1109/ACCESS.2019.2907131.

Zhang, S.; Zhang, S.; Wang, B.; Habetler, T.G. *Deep learning algorithms for bearing fault diagnostics - a comprehensive review.* IEEE Access, v. 8, p. 29857–29881, 2020. DOI: 10.1109/ACCESS.2020.2972859.

7. RESPONSIBILITY NOTICE

The authors are the only ones responsible for the printed material included in this paper.